

# Polymer-supported CuPd nanoalloy as a synergistic catalyst for electrocatalytic reduction of carbon dioxide to methane

Sheng Zhang<sup>a</sup>, Peng Kang<sup>a</sup>, Mohammed Bakir<sup>b</sup>, Alexander M. Lapides<sup>a</sup>, Christopher J. Dares<sup>a</sup>, and Thomas J. Meyer<sup>a,1</sup>

<sup>a</sup>Department of Chemistry, University of North Carolina at Chapel Hill, Chapel Hill, NC 27599; and <sup>b</sup>Department of Chemistry, University of the West Indies, Mona, Kingston 7, Jamaica

Contributed by Thomas J. Meyer, November 15, 2015 (sent for review October 13, 2015; reviewed by Hector Abruna and Amanda Morris)

**Developing sustainable energy strategies based on CO<sub>2</sub> reduction is an increasingly important issue given the world's continued reliance on hydrocarbon fuels and the rise in CO<sub>2</sub> concentrations in the atmosphere. An important option is electrochemical or photoelectrochemical CO<sub>2</sub> reduction to carbon fuels. We describe here an electrodeposition strategy for preparing highly dispersed, ultrafine metal nanoparticle catalysts on an electroactive polymeric film including nanoalloys of Cu and Pd. Compared with nanoCu catalysts, which are state-of-the-art catalysts for CO<sub>2</sub> reduction to hydrocarbons, the bimetallic CuPd nanoalloy catalyst exhibits a greater than twofold enhancement in Faradaic efficiency for CO<sub>2</sub> reduction to methane. The origin of the enhancement is suggested to arise from a synergistic reactivity interplay between Pd–H sites and Cu–CO sites during electrochemical CO<sub>2</sub> reduction. The polymer substrate also appears to provide a basis for the local concentration of CO<sub>2</sub> resulting in the enhancement of catalytic current densities by threefold. The procedure for preparation of the nanoalloy catalyst is straightforward and appears to be generally applicable to the preparation of catalytic electrodes for incorporation into electrolysis devices.**

solar energy | carbon dioxide reduction | CuPd nanoalloy | electropolymerized film | hydrocarbon

**D**eveloping sustainable energy resources and strategies to combat the hazards associated with the use of fossil fuels, which include global warming due to the increased concentration of greenhouse gases, is an important theme in the current energy and environmental research agenda (1–3). Electrochemical and photoelectrochemical CO<sub>2</sub> reduction to energy-dense hydrocarbon fuels could play a major role and become part of an integrated energy storage strategy, in combination with solar- or wind-generated electricity, as a way to store energy in the chemical bonds of carbon-based fuels (4–12). Metal-based catalysts for CO<sub>2</sub> reduction have been extensively studied over the last three decades. Metallic copper has proven to be the best available catalytic material for CO<sub>2</sub> reduction to hydrocarbons by electrochemical methods (13–19). Cu foils and single crystals have been extensively investigated but suffer from low surface areas, low catalytic current densities, and rapid deactivation during electrochemical CO<sub>2</sub> reduction (20). Recently, nanoparticle Cu catalysts (nanoCu) have been investigated as a way to increase catalytic current densities and stabilities. However, Faradaic efficiencies for electrocatalytic reduction to hydrocarbons decrease dramatically with particle size falling to ~10% for particles less than 20 nm in diameter. The size effect has been attributed to an enhanced chemisorption strength for CO at small Cu nanoparticles compared with large particles or bulk Cu electrodes (13). An additional complication arises from the use of surfactants in the syntheses of nanoCu because they can lead to significant contamination issues requiring their removal by a high-temperature posttreatment which causes adverse particle growth and loss of monodispersity (21).

Electrodeposition provides a facile and scalable technique for preparing catalytic electrodes. However, it can be difficult to control

and typically leads to large particle sizes, often from hundreds of nanometers to micrometers in diameter (22), resulting in low catalytic surface areas. We describe here a novel electrochemical method for synthesizing ultrafine metal nanoparticles and their application to CO<sub>2</sub> reduction. It is based on the use of an electropolymerized, electroactive film of a vinyl-2,2'-bipyridine complex of Fe(II). Following treatment with cyanide to displace a bpy ligand and coordinate cyanide, the Fe–CN groups provide a basis for binding metal ions from external solutions (21). After reduction of the film-incorporated metal ions to the corresponding metals, migration occurs to film surfaces where nanoparticles form with size control.

An outline for the overall procedure is shown in Fig. 1 for the surface-film-based reduction of Cu(II) to Cu(0). It involves in sequence: (i) Formation of a polymeric film of poly-[Fe(vbpy)<sub>3</sub>](PF<sub>6</sub>)<sub>2</sub> (vbpy is 4-methyl-4'-vinyl-2,2'-bipyridine) by electropolymerization induced by vbpy-based reduction. The electropolymerization procedure has been applied to polymer film formation on a variety of conductive substrates (23–26) including glassy carbon (GC) electrodes, planar fluorine-doped tin oxide (FTO) slides, reticulated vitreous carbon, and high surface area gas diffusion electrodes. (ii) Addition of cyanide ions which displaces a vbpy ligand from Fe(II) to give poly-Fe(vbpy)<sub>2</sub>(CN)<sub>2</sub>, poly-vbpy. (iii) Binding of Cu(II) ions from an external solution with coordination to the cyanide ligands. (iv) Electroreduction of the Cu(II) ions to give ultrafine nanoCu of uniform distribution on the surface of the polymeric film.

## Significance

**Photo- and electrochemical CO<sub>2</sub> reduction to carbon fuels is not only an attractive solution to the greenhouse effect, but could also become an integral part of a global energy storage strategy with renewable electrical energy sources used to store energy in the chemical bonds of carbon fuels. A novel electrodeposition strategy is reported here for the preparation of highly dispersed, ultrafine metal nanoparticles and nanoalloys on an electroactive polymeric film. It is shown that a bimetallic Cu–Pd nanoalloy exhibits a greater than twofold enhancement in Faradaic efficiency for CO<sub>2</sub> reduction to methane compared with a state-of-the-art nanoCu catalyst. The fabrication procedure for the alloy nanoparticles is straightforward and applicable as a general procedure for catalytic electrodes for integrated electrolysis devices.**

Author contributions: S.Z. and T.J.M. designed research; S.Z. and A.M.L. performed research; S.Z., P.K., M.B., C.J.D., and T.J.M. analyzed data; A.M.L. synthesized the complex; and S.Z., P.K., M.B., and T.J.M. wrote the paper.

Reviewers: H.A., Cornell University; and A.M., Virginia Tech.

The authors declare no conflict of interest.

<sup>1</sup>To whom correspondence should be addressed. Email: tjmeyer@unc.edu.

This article contains supporting information online at [www.pnas.org/lookup/suppl/doi:10.1073/pnas.1522496112/-DCSupplemental](http://www.pnas.org/lookup/suppl/doi:10.1073/pnas.1522496112/-DCSupplemental).

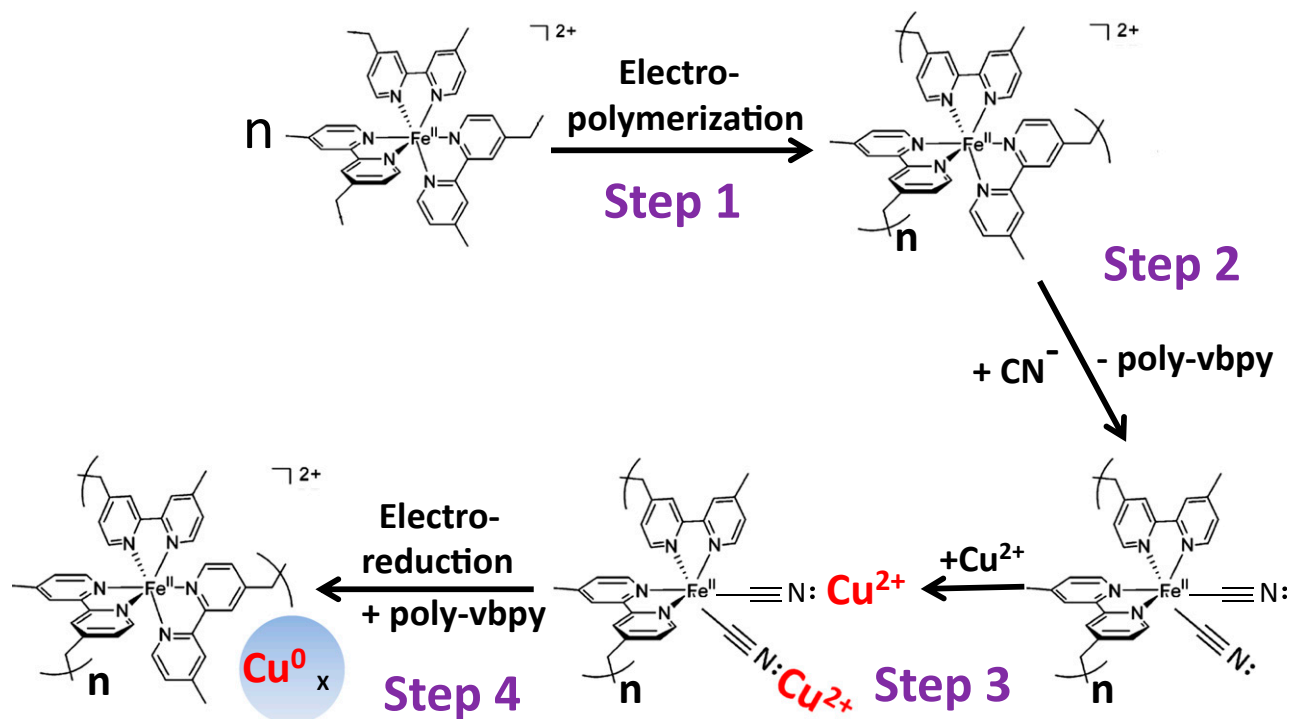


**Fig. 1.** Stepwise synthesis of nanoCu. Step 1: A polymeric film of poly-Fe(vbpy)<sub>3</sub>(PF<sub>6</sub>)<sub>2</sub> is preformed by reductive electropolymerization. Step 2: Cyanide displacement of a vbpy ligand gives the dicyano film poly-[Fe(vbpy)<sub>2</sub>(CN)<sub>2</sub>]<sub>poly-vbpy</sub>. Step 3: Metal ions Cu(II) are incorporated by binding to the cyanide ligands. Step 4: The bound metal ions are electrochemically reduced to metal nanoparticles.

The generality of the procedure is also demonstrated with an extension to the synthesis of polymeric films surface-loaded with nanoPd and with bimetallic CuPd nanoalloy. We demonstrate that the Cu-loaded films are electrocatalysts for CO<sub>2</sub> reduction to methane and that, compared with nanoCu, which, to date, is the best catalyst for

CO<sub>2</sub> reduction to hydrocarbons (13), the bimetallic CuPd nanoalloy provides an enhancement in Faradaic efficiency for CO<sub>2</sub> reduction to methane of >2 in both aqueous and organic solutions. The notable reactivity enhancement appears to arise from a synergistic mechanism involving Pd-H reduction of adsorbed CO from CO<sub>2</sub> reduction on Cu.

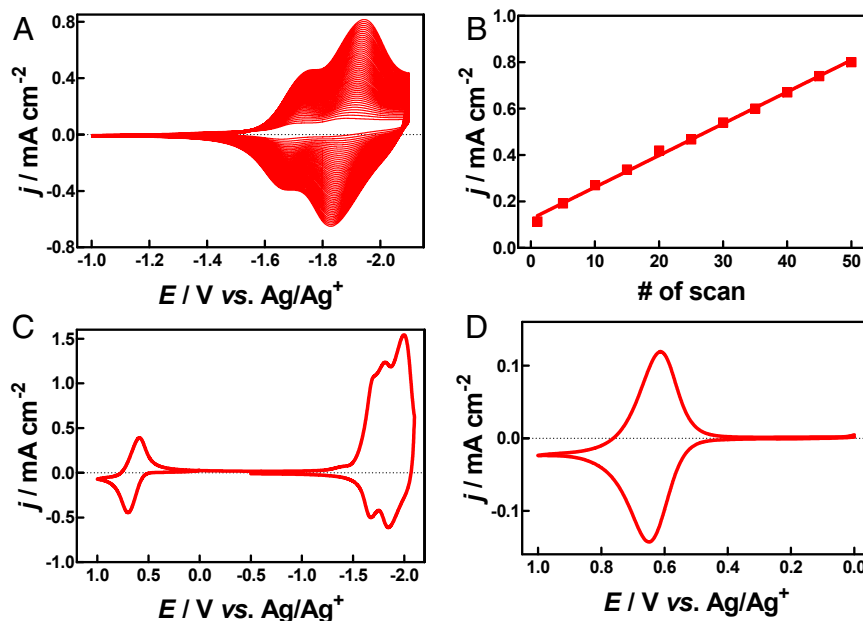


**Fig. 2.** (A) Reductive electropolymerization of [Fe(vbpy)<sub>3</sub>](PF<sub>6</sub>)<sub>2</sub> on a prepolished GC electrode by repetitive cycles at 100 mV/s between -1 and -2.1 V vs. Ag/AgNO<sub>3</sub> in 0.1 M TBAPF<sub>6</sub>/CH<sub>3</sub>CN containing 0.5 mM [Fe(vbpy)<sub>3</sub>](PF<sub>6</sub>)<sub>2</sub>. (B) Peak currents as a function of the number of scans for the electrode in Fig. 1A. (C) CVs of the final electrode at 50 mV/s following 30 cycles between -2.1 and 1 V vs. Ag/AgNO<sub>3</sub> in 0.1 M TBAPF<sub>6</sub>/CH<sub>3</sub>CN. (D) CV of the poly-[Fe(vbpy)<sub>3</sub>]<sup>3+/2+</sup> couple at 10 mV/s between 0 and 1 V vs. Ag/AgNO<sub>3</sub> in a fresh solution of 0.1 M TBAPF<sub>6</sub>/CH<sub>3</sub>CN.

## Results

**Preparation of poly-[Fe(vbpy)<sub>3</sub>](PF<sub>6</sub>)<sub>2</sub> Modified Electrodes.** Cyclic voltammetric (CV) scans at a GC electrode in a deaerated solution, 0.5 mM in Fe(vbpy)<sub>3</sub>(PF<sub>6</sub>)<sub>2</sub> in 0.1 M TBAPF<sub>6</sub>/CH<sub>3</sub>CN (TBA is tetrabutylammonium), between -1 and -2.1 V vs. Ag/AgNO<sub>3</sub> were performed. Surface waves corresponding to poly-[Fe(vbpy)<sub>3</sub>]<sup>2+/1+</sup> and poly-[Fe(vbpy)<sub>3</sub>]<sup>1+/0</sup> couples appear at -1.75 V and -1.95 V, respectively. As shown in Fig. 2A, peak currents increase with the number of scans. At these potentials, reduction of the vbpy ligands occurs, which induces vinyl polymerization (25, 27). The mechanism involves reduction and vinyl radical polymerization in the double layer near the electrode surface by C-C bond formation. With multiple polymerizable vinyl substituents, polymerization is accompanied by extensive cross-linking with insoluble pink polymeric films deposited on the electrode surface. The rate of film growth and resulting film thickness can be controlled by varying the concentration of complex in solution, the scan rate and potential range used in the preparative voltammetric scans, and the number of scan cycles. Under defined conditions, the incremental increase in polymer layer per scan is approximately constant as shown in Fig. 2B.

Surface stability and redox reactivity of the electropolymerized films were demonstrated by transferring a polymer-derivatized GC electrode to a fresh solution of the same electrolyte. CV scans indicated the appearance of stable waves for the poly-[Fe(vbpy)<sub>3</sub>]<sup>1+/0</sup>, poly-[Fe(vbpy)<sub>3</sub>]<sup>2+/1+</sup>, and poly-[Fe(vbpy)<sub>3</sub>]<sup>3+/2+</sup> surface couples, Fig. 2C, at -1.92V, -1.75 V, and 0.65 V vs. Ag/AgNO<sub>3</sub>. Surface coverages were estimated by integrating the charge under the [Fe(vbpy)<sub>3</sub>]<sup>3+/2+</sup> wave in Fig. 2D. Based on this analysis, the electroactive surface coverage was  $6 \times 10^{-9}$  mol cm<sup>-2</sup>, which corresponds to ~70 molecular layers with a monolayer surface coverage of  $\sim 8 \times 10^{-11}$  mol cm<sup>-2</sup> (see *SI Appendix*, Fig. S1 for details) (23). The resulting film thickness was ~300 nm as measured by scanning electron microscope (SEM) cross-sectional imaging, Fig. 3A. At this film thickness, with top-view images in Fig. 3B, the presence of spherical structures on the film surface (see *SI Appendix*, Fig. S2 for more SEM images), several micrometers in diameter, can be discerned. Similar morphologies have been observed for other

conductive polymers, including polypyrrole prepared by oxidative polymerization (28).

**Incorporation of Cu(II).** Soaking poly-Fe(vbpy)<sub>3</sub>(PF<sub>6</sub>)<sub>2</sub> films in 0.1 M tetrabutylammonium cyanide (TBACN)/CH<sub>3</sub>CN, resulted in rapid displacement of a single vbpy ligand to give poly-Fe(vbpy)<sub>2</sub>(CN)<sub>2</sub>, poly-vbpy evidenced by a visible color change from pink to purple which occurred on the time scale of minutes. Addition of the CN<sup>-</sup> ligands as coordination sites provides a basis for coordination and concentration of metal ions in the films (29). There was no evidence for further displacement of vbpy by CN<sup>-</sup> even over extended periods (24).

Exposure to external solutions containing 0.1 M Cu(OAc)<sub>2</sub> in CH<sub>3</sub>CN resulted in rapid incorporation of Cu(II) measured spectrophotometrically on optically transparent FTO electrodes, Fig. 3C (24). The changes in UV-visible spectra after incorporation of Cu(II) are consistent with Cu(II) binding to the CN<sup>-</sup> groups of the film-based complex (24). The visible absorption bands originate from  $d\pi(\text{Fe}^{\text{II}}) \rightarrow \pi^*(\text{bpy})$  metal-to-ligand charge-transfer transitions with replacement of coordinated poly-vbpy by CN<sup>-</sup> causing the shift to lower energy from 530 to 600 nm. Cyanide coordination is also consistent with the Raman spectral changes shown in *SI Appendix*, Fig. S3. Upon reduction of Cu(II) in the films to Cu(0) on the surface, the film absorbance maximum shifts back to ~530 nm, consistent with recoordination of the vbpy ligand to an Fe(II) center and loss of cyanide.

The proposed mechanism is consistent with both spectrophotometric results and electrochemical results on the polymeric films at the different stages in the synthesis, Fig. 3D. An Fe<sup>III/II</sup> wave appears at  $E_{1/2} = +0.7$  V vs. Ag/AgNO<sub>3</sub> for poly-[Fe(vbpy)<sub>3</sub>](PF<sub>6</sub>)<sub>2</sub> in the film. It shifts to  $E_{1/2} = +0.1$  V vs. Ag/AgNO<sub>3</sub> for the dicyano film, which is also consistent with CN<sup>-</sup> coordination to the Fe<sup>II</sup> sites in the films. In CVs of Cu(II)-incorporated films,  $E_{1/2}$  for Fe<sup>III/II</sup> couple shifts to +0.7 V vs. Ag/AgNO<sub>3</sub>, again consistent with Cu(II) binding to the CN<sup>-</sup> ligands in the adduct, and concurrent recoordination of a vbpy moiety by the Fe-based polymer.

**Metal Nanoparticles Preparation by Electroreduction.** Reduction of cyano-bound Cu(II) ions in the films by potential scans between

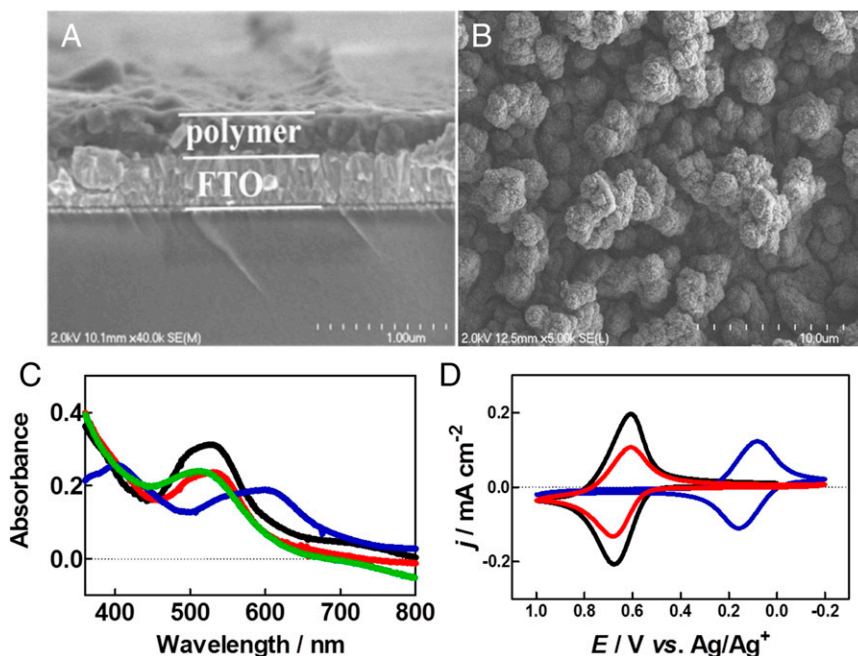


**Fig. 3.** SEM images: cross-section (A) and top view (B) of a poly-[Fe(vbpy)<sub>3</sub>](PF<sub>6</sub>)<sub>2</sub> film on an FTO slide. UV-visible spectra (C) and CVs (D) of poly-[Fe(vbpy)<sub>3</sub>](PF<sub>6</sub>)<sub>2</sub> (black), the dicyano film poly-[Fe(vbpy)<sub>2</sub>(CN)<sub>2</sub>], poly-vbpy (blue), the Cu(II) incorporated film (red), and the reduced Cu(0) incorporated film (green).

-1 and -1.6 V vs. Ag/AgNO<sub>3</sub> in 0.1 M TBACN/CH<sub>3</sub>CN resulted in the reduction of Cu(II) to Cu(0). Fig. 4A shows typical transmission electron microscope (TEM) images of the resulting nanoCu embedded in the film structure. They are ~7.8 nm in diameter and highly dispersed. Almost all of the Cu nanoparticles (*SI Appendix, Fig. S4*) were exposed on the polymeric film surface, and readily accessible to CO<sub>2</sub> in the electrolyte.

The impact of the CN<sup>-</sup> coordination strategy on particle dimensions was investigated by comparing the products of electrochemical reduction of CN<sup>-</sup> treated polymeric films of poly-[Fe(vbpy)<sub>3</sub>](PF<sub>6</sub>)<sub>2</sub> in 0.1 M TBAPF<sub>6</sub>/CH<sub>3</sub>CN on a planar FTO slide with a non-CN<sup>-</sup>-containing film. In the absence of cyanide, large, agglomerated Cu particles are produced (*SI Appendix, Figs. S5 and S6*) in marked contrast to the dispersed, ultrafine nanoparticles obtained when the film is pretreated with CN<sup>-</sup>.

In the dicyano films, a coordinated vbpy ligand in a poly-Fe(vbpy)<sub>3</sub>(PF<sub>6</sub>)<sub>2</sub> site is displaced by two CN<sup>-</sup> ligands followed by Cu(II) binding. Addition of CN<sup>-</sup> with coordination to Fe(II) occurs with high local homogeneity given the metal complex structure and initial reduction is homogeneously dispersed throughout the film structure. Following an initial reductive scan of Cu(II)-bound cyano films, Cu(0) appears and is dispersed throughout the film, initially with a continuing interaction with the cyanide ligands. At longer times Cu(0) aggregates form locally, initially as small Cu nanoclusters which diffuse to the surface of the films with formation of the ultrafine nanoCu (24).

The broader applicability of the cyanide coordination strategy was examined by the analogous synthesis of small, ultrafine nanoPd particles (~4.6 nm, *SI Appendix, Fig. S7*) shown in Fig. 4B and of bimetallic CuPd nanoalloy (~6.6 nm, *SI Appendix, Fig. S8*) in a 1:1 molar ratio (Fig. 4C). Diffraction peaks for bimetallic CuPd

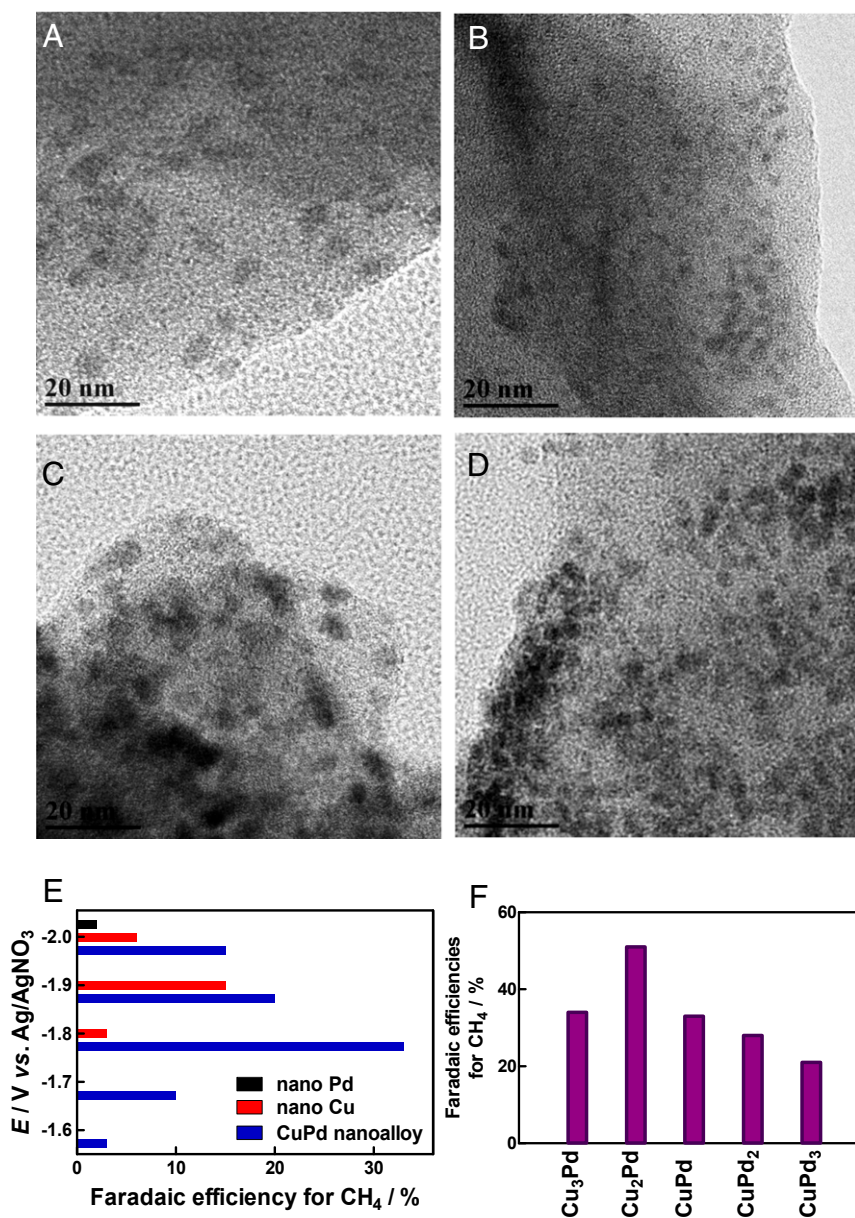


**Fig. 4.** Typical TEM images of nanoPd (A), nanoCu (B), CuPd nanoalloy (C), and Cu<sub>2</sub>Pd nanoalloy (D) on the polymeric film. (E) Plots of Faradaic efficiencies for methane production vs. applied potential on nanoCu, nanoPd, and CuPd nanoalloy. (F) Methane yields (recorded at -1.8 V vs. Ag/AgNO<sub>3</sub>) at Cu<sub>3</sub>Pd, Cu<sub>2</sub>Pd, CuPd, CuPd<sub>2</sub>, and CuPd<sub>3</sub> nanoalloy catalysts. CO<sub>2</sub> reduction was performed in CO<sub>2</sub>-saturated 0.1 M TBAPF<sub>6</sub>/CH<sub>3</sub>CN solutions with 1 M added H<sub>2</sub>O.

nanocatalyst in *SI Appendix, Fig. S9* can be indexed as (111), (200), (220), and (311) reflections for the fcc structure for the CuPd nanoalloy. For both the Cu- and nanoalloy-containing films, retention of the Fe(II) in the films was shown by UV-visible absorption measurements.

These results suggest that the polymer film/coordination/reduction strategy may provide a general electrochemical procedure for synthesizing ultrafine, monodispersed metal nanoparticles on/imbedded in an electroactive polymer film without the use of surfactants.

**Electrocatalytic Reduction of CO<sub>2</sub> to Methane.** The electrocatalytic reactivity of the nanoparticle films on a GC electrode toward CO<sub>2</sub> reduction was evaluated by controlled potential electrolysis in CO<sub>2</sub>-saturated 0.1 M TBAPF<sub>6</sub>/CH<sub>3</sub>CN solutions with 1 M added H<sub>2</sub>O. The mixed solvent strategy exploits the higher CO<sub>2</sub> solubility in CH<sub>3</sub>CN, which is ~eightfold greater than in water (30). The products of CO<sub>2</sub> reduction were analyzed by both <sup>1</sup>H NMR in the liquid phase and by GC in the headspace. Results of the electrolyses at CuPd nanoalloys, nanoCu, and nanoPd are summarized in *SI Appendix, Table S1*. Catalytic currents were stable over extended electrolysis periods as shown in *SI Appendix, Fig. S17*. The products of electrolysis were CH<sub>4</sub>, CO, and H<sub>2</sub>.

The 8e<sup>-</sup>/8H<sup>+</sup> product, CH<sub>4</sub>, is the most highly reduced product. The ultrafine nanoCu catalyst produced CH<sub>4</sub> with 15% Faradaic yield, which is comparable to previous reports (13). A notably enhanced catalytic reactivity toward reduction to CH<sub>4</sub> is observed for the CuPd nanoalloy. No CH<sub>4</sub> was detected at poly-[Fe(vbpy)<sub>3</sub>](PF<sub>6</sub>)<sub>2</sub> film under the same conditions. Fig. 4E shows potential-dependent Faradaic efficiencies for CH<sub>4</sub> produced at ultrafine nanoCu, nanoPd, and bimetallic CuPd nanoalloy. The maximum Faradaic efficiency for CH<sub>4</sub> of 33% was achieved for the bimetallic CuPd nanoalloy, a doubling of yield compared with nanoCu. Moreover, the onset for CO<sub>2</sub> reduction to CH<sub>4</sub> at CuPd nanoalloy appears at ~-1.6 V vs. Ag/AgNO<sub>3</sub> (an overpotential of 0.66 V for the CO<sub>2</sub>/CH<sub>4</sub> couple; see *SI Appendix, Table S1* for details), which is ~400 mV more positive than at nanoPd and ~200 mV more positive than at nanoCu.

As shown in *SI Appendix, Fig. S17*, compared with carbon black as the electrode substrate (*SI Appendix, Fig. S18*), the polymer-film-supported CuPd nanoalloy exhibited an enhanced current density by a factor of ~3 (~6 mA cm<sup>-2</sup>) compared with nanoCu under the same electrolysis conditions. This may be a consequence of the concentration of the active catalyst on the film surface and of enhanced local concentration of CO<sub>2</sub> in the polymer film (31).

The effect of alloy composition on Faradaic efficiencies for CH<sub>4</sub> production was investigated systematically by use of series of Cu/Pd nanoalloy samples with varying ratios of Cu and Pd from 3:1–1:3. TEM images and size-distribution histograms are shown in *SI Appendix, Figs. S10–S13*. Their reactivities toward CO<sub>2</sub> reduction were first investigated in CO<sub>2</sub>-saturated 0.1 M TBAPF<sub>6</sub>/CH<sub>3</sub>CN solutions with 1 M added H<sub>2</sub>O. Methane yields as a function of composition in Fig. 4F show that the maximum Faradaic efficiency (51%) for methane is found to occur for the Cu<sub>2</sub>Pd nanoalloy shown in Fig. 4D with a rationale discussed below.

Aqueous CO<sub>2</sub> reduction activities have been also evaluated at the optimal Cu<sub>2</sub>Pd nanoalloy and compared with nanoCu as a catalyst in 0.1 M KHCO<sub>3</sub> aqueous solutions by controlled potential electrolysis at -1.68 V vs. SCE. Under these conditions the methane yield is 36% for the Cu<sub>2</sub>Pd nanoalloy compared with 13% for the nanoCu catalyst, demonstrating a significant enhancement toward CO<sub>2</sub> reduction to CH<sub>4</sub> in both aqueous and organic solvents with an intrinsically higher reactivity for the nanoalloy. The methane yield was further enhanced to 48% by electrolysis in aqueous solution at 0 °C. The Cu<sub>2</sub>Pd nanoalloy catalysts have methane yields that are comparable to bulk Cu electrodes but with significantly enhanced stability toward degradation

in the rate of methane production with time (see *SI Appendix, Fig. S14* for details).

## Discussion

To gain mechanistic insight into electrocatalytic CO<sub>2</sub> reduction at the bimetallic catalyst, partial current density Tafel plots for CO<sub>2</sub> reduction to CH<sub>4</sub> at CuPd nanoalloy and nanoCu are compared in *SI Appendix, Fig. S15*. The Tafel slope for CuPd nanoalloy is calculated to be 70 mV dec<sup>-1</sup>, which is consistent with a mechanism involving a chemical rate-determining step (RDS) (5). In earlier studies on CO<sub>2</sub> reduction to methane at Cu, Hori et al. concluded that the RDS involved an adsorbed CO reaction step (32, 33). Hydride reduction of transition metal bound or free CO is a well-known reaction (34–37). A reasonable suggestion for the appearance of CH<sub>4</sub> on the CuPd nanoalloy is that the rate-limiting Pd–H reduction of adsorbed CO occurs following CO<sub>2</sub> reduction to CO at Cu.

We have explored this reactivity with the electrochemically generated hydride Ru(tpy)(bpy)H<sup>+</sup> as a homogeneous catalyst. It is generated in situ by electrochemical reduction of Ru(tpy)(bpy)(NCMe)<sup>2+</sup> in MeCN with added water at potentials more negative than -1.95 V vs. Ag/AgNO<sub>3</sub> as described in our previous report (38). As shown in *SI Appendix, Fig. S16A*, addition of the Ru(II) complex at a nanoCu electrode resulted in catalytic current enhancement. In the differential pulse voltammetry curve in *SI Appendix, Fig. S16B*, reduction peaks at -1.55 V and -1.88 V vs. Ag/AgNO<sub>3</sub> appear due to sequential one-electron reductions at tpy followed by one-electron bpy reduction (38). *SI Appendix, Fig. S16C* shows that, with added complex, the methane yield increases from 6% to 16% at an applied potential of -2 V, conditions known to reduce the nitrile complex to the hydride. Under these conditions, the CO yield decreased from 16% to 8%. Electrolysis at -1.8 V, without reduction to the hydride, results in essentially no change in the methane yield, 4% vs. 3%. These results are consistent with facilitation of methane formation by the electrogenerated hydride, presumably by reduction of surface-bound CO.

Hori et al. reported that during CO<sub>2</sub> electroreduction at Cu foil electrodes, about 90% of the Cu surface area was covered by adsorbed CO from reduction of CO<sub>2</sub> (32). Small Cu nanoparticles have stronger chemisorption binding strengths to CO than large particles or bulk Cu (13) and the surface of the nanoCu catalyst is presumably covered by adsorbed CO, resulting in the very low methane yields (~10%) observed at nanoCu. For the CuPd nanoalloy, Pd-hydride sites generated in situ presumably facilitate the reduction of CO adsorbed at Cu sites to methane. The maximum methane yield is achieved for the Cu<sub>2</sub>Pd nanoalloy. Catalysts with a higher Cu ratio, Cu<sub>3</sub>Pd, produce more CO, whereas more hydrogen is generated at samples higher in Pd (CuPd, CuPd<sub>2</sub>, and CuPd<sub>3</sub>).

Relatively high methane yields (over 50%) have been obtained at bulk Cu electrodes but they suffer from severe poisoning and deactivation during CO<sub>2</sub> reduction (20). Deactivation originates from the deposition of heavy metal impurities in the electrolyte and from the formation of graphitic carbon on Cu electrode surfaces (20). Metal impurities in the electrolyte have been removed by preelectrolysis (20), but the formation of graphitic hydrocarbons continues with hydrogen evolution increasing at the expense of CO<sub>2</sub> reduction within an hour after initiation of electrolysis. The change in products is mainly due to the formation of a graphitic carbon layer which prevents CO<sub>2</sub> reduction (39, 40). In contrast, nanostructured Cu catalysts have been found to be stable over 5 h of CO<sub>2</sub> electrolysis, with the increase attributed to the higher surface areas at the nanoparticle catalysts (19, 41). The production rate of methane at the CuPd nanoalloy catalyst remains stable over 3 h of CO<sub>2</sub> electrolysis, which is a notable observation. This catalyst has the dual advantages of relatively high methane yield, comparable to bulk Cu, but with significantly enhanced long-term performance.

We report here a film-based cyanide coordination protocol for templated electrochemical reduction of bound metal ions, Cu(II), Pd(II), which upon reduction, give uniform, ultrafine metal nanoparticles on the surfaces of conductive, electropolymerized films. The procedure, with electroreduction of homogeneously dispersed, chemically bound metal ions, results in the formation of metallic nanoclusters on the film surfaces. It provides what could become a broad, general approach for the synthesis of nanoscale metal and metal alloy particles on electroactive substrates. It is notable that the cyanide-film strategy described here is facile and general and amenable to scale up with the possibility of using of gas diffusion electrodes to achieve high current densities and efficiencies for CO<sub>2</sub> reduction.

Simultaneous coordination of Cu(II) and Pd(II) followed by reduction results in a CuPd nanoalloy with enhanced Faradaic efficiency and a decrease in onset potential for electrocatalytic CO<sub>2</sub> reduction to methane. An optimized Faradaic efficiency for CH<sub>4</sub> production of 51% was obtained at a Cu<sub>2</sub>Pd nanoalloy. The

origin of the bimetallic synergistic effect appears to lie in the rate-limiting Pd–H reduction of Cu-bound CO. This finding provides new insights into CO<sub>2</sub> reduction with design and control of product distribution by varying alloy composition and solution conditions. The use of an external, homogeneous cocatalyst for hydride formation and enhanced CO<sub>2</sub> reduction to methane is also a notable observation, one that could presage a general, integrated heterogeneous/homogeneous catalytic strategy for CO<sub>2</sub> reduction and other reactions in the future.

**ACKNOWLEDGMENTS.** We thank Dr. Amar Kumbhar and Dr. Carrie Donley (CHANL) for assistance with SEM, TEM, and X-ray photoelectron spectra measurements. This research was supported solely by the UNC EFRC: Center for Solar Fuels, an Energy Frontier Research Center funded by the US Department of Energy Office of Science, Office of Basic Energy Sciences under Award DE-SC0001011. A.M.L. acknowledges a graduate fellowship supported by the Department of Defense through the National Defense Science & Engineering Graduate Fellowship Program.

1. Rosen BA, et al. (2011) Ionic liquid-mediated selective conversion of CO<sub>2</sub> to CO at low overpotentials. *Science* 334(6056):643–644.
2. Costentin C, Drouot S, Robert M, Savéant J-M (2012) A local proton source enhances CO<sub>2</sub> electroreduction to CO by a molecular Fe catalyst. *Science* 338(6103):90–94.
3. Li CW, Ciston J, Kanan MW (2014) Electroreduction of carbon monoxide to liquid fuel on oxide-derived nanocrystalline copper. *Nature* 508(7497):504–507.
4. Hori Y (2008) Electrochemical CO<sub>2</sub> reduction on metal electrodes. *Modern Aspects of Electrochemistry*, eds Vayenas C, White R, Gamboa-Aldeco M (Springer, New York), Vol 42, pp 89–189.
5. Zhang S, Kang P, Meyer TJ (2014) Nanostructured tin catalysts for selective electrochemical reduction of carbon dioxide to formate. *J Am Chem Soc* 136(5):1734–1737.
6. Kang P, Zhang S, Meyer TJ, Brookhart M (2014) Rapid selective electrocatalytic reduction of carbon dioxide to formate by an iridium pincer catalyst immobilized on carbon nanotube electrodes. *Angew Chem Int Ed* 126(33):8853–8857.
7. Chen Z, et al. (2012) Splitting CO<sub>2</sub> into CO and O<sub>2</sub> by a single catalyst. *Proc Natl Acad Sci USA* 109(39):15606–15611.
8. Zhu W, et al. (2013) Monodisperse Au nanoparticles for selective electrocatalytic reduction of CO<sub>2</sub> to CO. *J Am Chem Soc* 135(45):16833–16836.
9. Kim D, Resasco J, Yu Y, Asiri AM, Yang P (2014) Synergistic geometric and electronic effects for electrochemical reduction of carbon dioxide using gold-copper bimetallic nanoparticles. *Nat Commun* 5:4948.
10. Kumar B, et al. (2013) Renewable and metal-free carbon nanofiber catalysts for carbon dioxide reduction. *Nat Commun* 4:2819.
11. Lu Q, et al. (2014) A selective and efficient electrocatalyst for carbon dioxide reduction. *Nat Commun* 5:3242.
12. Kas R, et al. (2014) Electrochemical CO<sub>2</sub> reduction on Cu<sub>2</sub>O-derived copper nanoparticles: Controlling the catalytic selectivity of hydrocarbons. *Phys Chem Chem Phys* 16(24):12194–12201.
13. Reske R, Mistry H, Beharfarid F, Roldan Cuenya B, Strasser P (2014) Particle size effects in the catalytic electroreduction of CO<sub>2</sub> on Cu nanoparticles. *J Am Chem Soc* 136(19):6978–6986.
14. Kuhl KP, et al. (2014) Electrocatalytic conversion of carbon dioxide to methane and methanol on transition metal surfaces. *J Am Chem Soc* 136(40):14107–14113.
15. Peterson AA, Abild-Pedersen F, Studt F, Rossmeisl J, Nørskov JK (2010) How copper catalyzes the electroreduction of carbon dioxide into hydrocarbon fuels. *Energy Environ Sci* 3(9):1311–1315.
16. Nie X, Esopi MR, Janik MJ, Asthagiri A (2013) Selectivity of CO<sub>2</sub> reduction on copper electrodes: The role of the kinetics of elementary steps. *Angew Chem Int Ed Engl* 52(9):2459–2462.
17. Hori Y, Takahashi R, Yoshinami Y, Murata A (1997) Electrochemical reduction of CO at a copper electrode. *J Phys Chem B* 101(36):7075–7081.
18. Manthiram K, Beberwyck BJ, Alivisatos AP (2014) Enhanced electrochemical methanation of carbon dioxide with a dispersible nanoscale copper catalyst. *J Am Chem Soc* 136(38):13319–13325.
19. Roberts FS, Kuhl KP, Nilsson A (2015) High selectivity for ethylene from carbon dioxide reduction over copper nanocube electrocatalysts. *Angew Chem Int Ed Engl* 54(17):5179–5182.
20. Hori Y, et al. (2005) “Deactivation of copper electrode” in electrochemical reduction of CO<sub>2</sub>. *Electrochim Acta* 50(27):5354–5369.
21. Peng Z, Kisielowski C, Bell AT (2012) Surfactant-free preparation of supported cubic platinum nanoparticles. *Chem Commun (Camb)* 48(13):1854–1856.
22. Chen Z, Kang P, Zhang M-T, Stoner BR, Meyer TJ (2013) Cu(II)/Cu(0) electrocatalyzed CO<sub>2</sub> and H<sub>2</sub>O splitting. *Energy Environ Sci* 6(3):813–817.
23. Abruna HD, Meyer TJ, Murray RW (1979) Chemical and electrochemical properties of 2,2'-bipyridyl complexes of ruthenium covalently bound to platinum oxide electrodes. *Inorg Chem* 18(11):3233–3240.
24. Bakir M, MacKay SG, Linton RW, Sullivan BP, Meyer TJ (1994) Binding and reduction of silver ions in thin polymeric films of poly-[Fe(vbpy)<sub>2</sub>(CN)<sub>2</sub>]<sub>n</sub>-poly-vbpy. *Inorg Chem* 33(18):3945–3951.
25. Calvert JM, et al. (1983) Synthetic and mechanistic investigations of the reductive electrochemical polymerization of vinyl-containing complexes of iron(II), ruthenium(II), and osmium(II). *Inorg Chem* 22(15):2151–2162.
26. Lapidés AM, et al. (2013) Stabilization of a ruthenium(II) polypyridyl dye on nanocrystalline TiO<sub>2</sub> by an electropolymerized overlayer. *J Am Chem Soc* 135(41):15450–15458.
27. Ghosh P, Spiro TG (1980) Photoelectrochemistry of tris(bipyridyl)ruthenium(II) covalently attached to n-type tin(IV) oxide. *J Am Chem Soc* 102(17):5543–5549.
28. Zhang S, Shao Y, Liu J, Aksay IA, Lin Y (2011) Graphene-polypyrrole nanocomposite as a highly efficient and low cost electrically switched ion exchanger for removing ClO<sub>4</sub><sup>-</sup> from wastewater. *ACS Appl Mater Interfaces* 3(9):3633–3637.
29. Torelli DA, Harrison DP, Lapidés AM, Meyer TJ (2013) Strategies for stabilization of electrodeposited metal particles in electropolymerized films for H<sub>2</sub>O oxidation and H<sup>+</sup> reduction. *ACS Appl Mater Interfaces* 5(15):7050–7057.
30. Tomita Y, Teruya S, Koga O, Hori Y (2000) Electrochemical reduction of carbon dioxide at a platinum electrode in acetonitrile-water mixtures. *J Electrochem Soc* 147(11):4164–4167.
31. Yan Y, Zeitler EL, Gu J, Hu Y, Bocarsly AB (2013) Electrochemistry of aqueous pyridinium: Exploration of a key aspect of electrocatalytic reduction of CO<sub>2</sub> to methanol. *J Am Chem Soc* 135(38):14020–14023.
32. Hori Y, Murata A, Yoshinami Y (1991) Adsorption of CO, intermediately formed in electrochemical reduction of CO<sub>2</sub>, at a copper electrode. *J Chem Soc, Faraday Trans* 87(1):125–128.
33. Hori Y, Murata A, Takahashi R (1989) Formation of hydrocarbons in the electrochemical reduction of carbon dioxide at a copper electrode in aqueous solution. *J Chem Soc, Faraday Trans* 85(8):2309–2326.
34. Lapinte C, Catheline D, Astruc D (1988) Sodium borohydride reduction of carbon monoxide in the cationic iron carbonyl complexes [C<sub>5</sub>Me<sub>5</sub>Fe(CO)<sub>2</sub>]<sup>+</sup>PF<sub>6</sub><sup>-</sup> (L=CO or phosphine). *Organometallics* 7(8):1683–1691.
35. Muetterties EL, Stein J (1979) Mechanistic features of catalytic carbon monoxide hydrogenation reactions. *Chem Rev* 79(6):479–490.
36. Sweet JR, Graham WAG (1982) Stepwise reduction of coordinated carbon monoxide. *J Am Chem Soc* 104(10):2811–2815.
37. Wolczanski PT, Bercaw JE (1980) Mechanisms of carbon monoxide reduction with zirconium hydrides. *Acc Chem Res* 13(4):121–127.
38. Chen Z, Glasson CRK, Holland PL, Meyer TJ (2013) Electrogenated polypyridyl ruthenium hydride and ligand activation for water reduction to hydrogen and acetone to iso-propanol. *Phys Chem Chem Phys* 15(24):9503–9507.
39. DeWulf DW, Jin T, Bard AJ (1989) Electrochemical and surface studies of carbon dioxide reduction to methane and ethylene at copper electrodes in aqueous solutions. *J Electrochem Soc* 136(6):1686–1691.
40. Wasmus S, Cattaneo E, Vielstich W (1990) Reduction of carbon dioxide to methane and ethene—an on-line MS study with rotating electrodes. *Electrochim Acta* 35(4):771–775.
41. Li CW, Kanan MW (2012) CO<sub>2</sub> reduction at low overpotential on Cu electrodes resulting from the reduction of thick Cu<sub>2</sub>O films. *J Am Chem Soc* 134(17):7231–7234.